Rapid Communications

Fermions and bosons in nonsymmorphic $PdSb_2$ with sixfold degeneracy

Ramakanta Chapai,[1] Yating Jia,[2] W. A. Shelton,[3] Roshan Nepal,[1] Mohammad Saghayezhian,[1] J. F. DiTusa,[1] E. W. Plummer,[1] Changqing Jin,[2,*] and Rongying Jin[1,†]

[1]*Department of Physics and Astronomy, Louisiana State University, Baton Rouge, Louisiana 70803, USA*

[2]*Institute of Physics; School of Physics, University of Chinese Academy of Sciences, Chinese Academy of Science, Beijing, 100190, China*

[3]*Cain Department of Chemical Engineering, Louisiana State University, Baton Rouge, Louisiana 70803, USA*

(Received 25 July 2018; published 16 April 2019)

$PdSb_2$ is a candidate for hosting sixfold-degenerate exotic fermions (beyond Dirac and Weyl fermions). The nontrivial band crossing protected by the nonsymmorphic symmetry plays a crucial role in physical properties. We have grown high-quality single crystals of $PdSb_2$ and characterized their physical properties under several stimuli (temperature, magnetic field, and pressure). While it is a diamagnetic Fermi-liquid metal under ambient pressure, $PdSb_2$ exhibits a large magnetoresistance with continuous increase up to 14 T, which follows Kohler's scaling law at all temperatures. This implies one-band electrical transport, although multiple bands are predicted by first-principles calculations. By applying magnetic field along the [111] direction, de Haas–van Alphen oscillations are observed with frequency of 102 T. The effective mass is nearly zero ($0.045m_0$) with the Berry phase close to π, confirming that the band close to the R point has a nontrivial character. Under quasihydrostatic pressure (p), evidence for superconductivity is observed in the resistivity below the critical temperature T_c. The dome-shaped T_c versus p is obtained with maximum $T_c^{\max} \sim 2.9$ K. We argue that the formation of Cooper pairs (bosons) is the consequence of the redistribution of the sixfold-degenerate fermions under pressure.

DOI: 10.1103/PhysRevB.99.161110

The discovery of topological properties in condensed matter started a new era of physics. Many fermionic particles and phenomena predicted in high-energy physics are now experimentally observed in topological materials such as Dirac, Weyl, and Majorana particles [1–3]. Their nontrivial topology gives rise to exotic physical properties, opening the door to future electronics with low-power consumption. The nontrivial topology results from crossings of conduction and valence bands. Depending on crystal symmetry, such crossings can result in degeneracy (g) with $g = 2$, 3, 4, 6, and 8. It is known that $g = 2$ corresponds to Weyl fermions and $g = 4$ corresponds to Dirac fermions. These fermions have been extensively studied both in condensed-matter physics and high-energy physics [4–9]. The cases of $g = 3$, 6, and 8 are particularly interesting as they can only be found in condensed-matter systems, having no high-energy analogs as constrained by Poincaré symmetry [10].

Based on the density-functional theory (DFT), $PdSb_2$ is predicted to have $g = 6$, where the degeneracy is stabilized by its nonsymmorphic symmetry: $Pa\bar{3}$ [10]. In this space group, there arises threefold degeneracy, which is doubled by the presence of time-reversal symmetry resulting in *sixfold degeneracy*. For $PdSb_2$, the sixfold degeneracy occurs at the time-reversal invariant R point at the corner of the Brillouin zone. Unlike Dirac and Weyl bands with linear dependence with energy, the sixfold-degenerate bands at the R point have quadratic energy dependence [10]. However, non-Abelian Berry curvature is expected under special holonomy [10]. Although $PdSb_2$ has been structurally characterized in the early 1960s [11], its physical properties remain unknown [12]. We have grown $PdSb_2$ single crystals, confirming its nonsymmorphic structure. We report its electrical and magnetic properties under various stimuli [temperature (T), magnetic field (H), and quasihydrostatic pressure (p)]. Several interesting properties are discovered: (1) $PdSb_2$ is a diamagnetic metal with the Fermi-liquid ground state under ambient pressure; (2) there is large positive magnetoresistance (MR) without sign of saturation up to 14 T, which obeys Kohler's scaling law; (3) there are de Haas–van Alphen oscillations with frequency of 102 T when field is applied along the [111] direction, revealing nearly zero effective electron mass and a nontrivial Berry phase; (4) it becomes superconducting under the application of p with the maximum superconducting transition temperature at $T_c^{\max} \sim 2.9$ K; and (5) first-principles calculations indicate the change of band structure under pressure, leading to the charge redistribution.

$PdSb_2$ single-crystal growth and phase determination are described in Ref. [13]. All x-ray diffraction (XRD) peaks can be indexed under a pyrite-type cubic structure [space group 205 ($Pa\bar{3}$)] with the lattice parameter 6.464 Å [Supplemental Material, Fig. S1(a) [13]), consistent with the previously reported value [14]. The magnetization measurements were performed in a magnetic property measurement system (MPMS) (Quantum Design). At ambient pressure, the electrical properties were measured using the standard four-probe technique in a physical property measurement system (PPMS)-14 T (Quantum Design). The resistivity under quasihydrostatic pressure was measured via the four-probe method using a diamond-anvil cell as described in Refs. [13,15–17]. DFT calculations were performed using a plane-wave-based approach that

*Jin@iphy.ac.cn
†rjin@lsu.edu

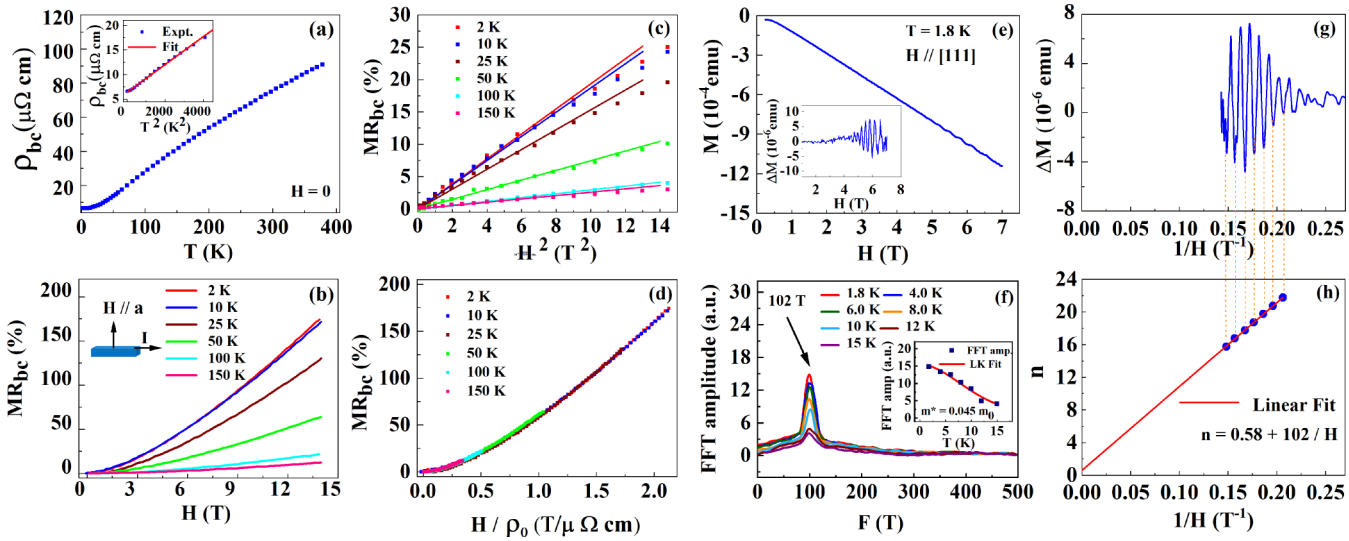

FIG. 1. (a) Temperature dependence of the electrical resistivity (ρ_{bc}) of $PdSb_2$. Inset: ρ_{bc} versus T^2 and fit with $\rho = \rho_0 + AT^2$ below 60 K; (b) transverse MR_{bc} at indicated temperatures; (c) MR_{bc} versus H^2 below 4 T; (d) Kohler plot at indicated temperatures; (e) magnetization versus field at 1.8 K with $H//[111]$. Inset: ΔM after background subtraction; and (f) FFT of oscillatory ΔM at indicated temperatures. Inset: Temperature dependence of FFT amplitude and its fit to the Lifshitz-Kosevich formula (see text); (g) ΔM plotted as a function of H^{-1}; (h) Landau fan diagram constructed from ΔM at 1.8 K. The solid line is the fit of the data using the Onsager equation.

incorporates the projected-augmented wave method within the Vienna *Ab initio* Simulation Package (VASP) [13,18–21].

Figure 1(a) shows the temperature dependence of the electrical resistivity of $PdSb_2$ along the *bc* plane (ρ_{bc}). Note ρ_{bc} decreases with decreasing temperature between 2 and 400 K with $\rho_{bc}(300\,\mathrm{K}) \sim 75.9\,\mu\Omega\,\mathrm{cm}$ and $\rho_{bc}(2\,\mathrm{K}) \sim 6.6\,\mu\Omega\,\mathrm{cm}$, indication of good metallicity. At low temperatures, the data can be fitted with $\rho_{bc}(T) = \rho_0 + AT^2$ below 60 K with $\rho_0 = 6.4\,\mu\Omega\,\mathrm{cm}$ and $A = 2.8\,\mathrm{n}\Omega\,\mathrm{cm\,K^{-2}}$ [see inset of Fig. 1(a)]. The T^2 dependence of ρ_{bc} in this nonmagnetic system indicates the Fermi-liquid ground state with dominant electron-electron scattering at low temperatures.

$PdSb_2$ is diamagnetic resulting from atom core contributions (Fig. S1(c) [13]). Applying H either parallel or perpendicular to the current I, we find that there is positive MR. Figure 1(b) displays the transverse ($H \perp I$) MR_{bc} at indicated temperatures. The MR_{bc} increases with decreasing temperature. At a fixed temperature, the MR increases with increasing field without any sign of saturation, reaching 174% at 2 K and 14 T. For $H//I$, the MR_{bc} is about one order of magnitude smaller (Fig. S2 [13]).

Since the MR_{bc} for $H//I$ is much smaller than that for $H \perp I$, there is little contribution from spin scattering. The positive MR in a nonmagnetic metallic system is attributed to the modification of electron trajectories due to the application of H. This effect is more significant at low temperatures in pure metallic systems where charge carriers effectively follow the cyclotron motion around the magnetic field [22–25]. By plotting MR_{bc} versus H^2 in Fig. 1(c), we find that the MR_{bc} displays quadratic field dependence in the low-field regime (<3 T), as expected for conventional metals with a single band. At higher fields, MR_{bc} gradually deviates from H^2 dependence, while continuously increasing. Such a nonsaturating MR has been attributed to exotic mechanisms. For example, MR for the nonsymmorphic Dirac semimetal Cd_3As_2 continuously increases up to 65 T, which is attributed to mobility fluctuations [26]. The MR of Cd_3As_2 also scales with H/ρ_0 [26], indicating an effective single-band transport. For $PdSb_2$, the MR_{bc} data taken at different temperatures collapse into a single curve when plotting MR_{bc} versus H/ρ_0 as shown in Fig. 1(d). This implies that Kohler's law is valid for $PdSb_2$ as well, which is for a single-band transport scenario [25,26]. Although calculations (Fig. 2 and Ref. [10]) indicate the multiband nature of $PdSb_2$, it appears that only one band plays a dominant role in electrical transport. In fact, the effective single-band transport in multiband systems is a common feature of topological materials [26].

While there is no sign for quantum oscillations when field is applied along the principal axes of crystals, we have observed such oscillations when the magnetization (M) is measured along the high-symmetry Γ-R direction. Figure 1(e) shows the H dependence of M along the [111] direction at 1.8 K, which exhibits oscillatory behavior with increasing H. The magnetization ΔM after subtracting a smooth background is shown in the inset of Fig. 1(e). The application of a fast Fourier transformation (FFT) to ΔM yields a single frequency $F = 102\,\mathrm{T}$ [Fig. 1(f)] for all temperatures. The FFT amplitude decreases with increasing temperature. The temperature dependence of the FFT amplitude is used to determine the effective mass m^* of electrons residing in this Fermi surface using the Lifshitz-Kosevich equation [27] $\mathrm{FFT}(T) = \frac{A'(\frac{m^*}{m_0})T}{\sinh(A'(\frac{m^*}{m_0})T)}$ ($A' = \frac{2\pi^2 k_B m_0}{e\hbar\bar{H}}$, m_0 is the free-electron mass, and $\bar{H}$ is the average magnetic field for our applied field range). The fit of this equation to our data yields $m* = 0.045 m_0$. This value is close to what is obtained in Cd_3As_2 [26] and Weyl semimetal $BaMnSb_2$ [7].

The same frequency is obtained if ΔM is plotted as a function of $1/H$ as displayed in Fig. 1(g). Based on the observed oscillations, the Landau fan diagram can be constructed by assigning the minimum ΔM to $n - 1/4$ [28], where n is the

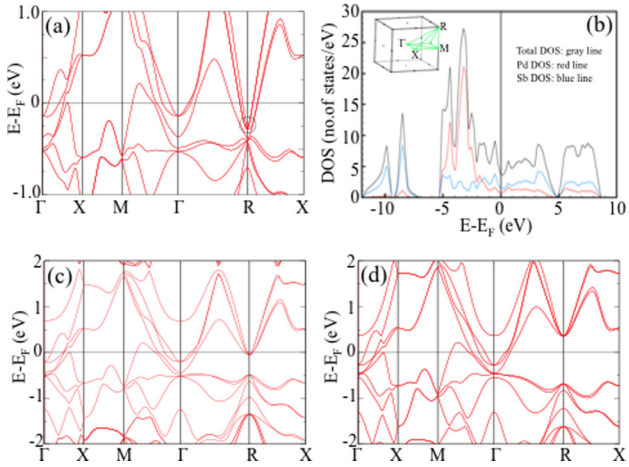

FIG. 2. (a) Electronic structure near the Fermi level. (b) DOS from Pd (red), Sb (blue), and the sum. Inset: First Brillouin zone of $PdSb_2$. (c), (d) Band structure under $p = 17.66$ and 45.60 GPa, respectively.

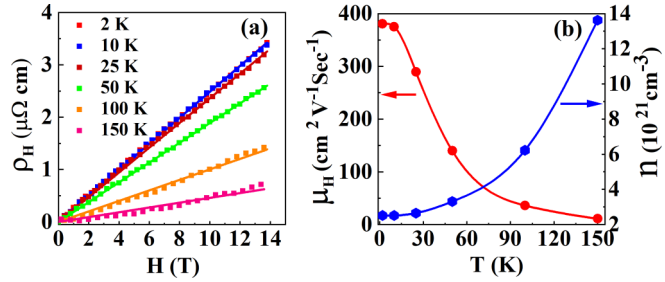

FIG. 3. (a) Hall resistivity ρ_H measured at different temperatures and corresponding linear fits (solid lines). (b) Temperature dependence of the Hall mobility μ_H (red) and carrier concentration n (blue).

Landau-level index. As shown in Fig. 1(h), $n(H^{-1})$ can be described as $n = 0.58 + 102/H$. This implies that $\Phi_{\text{Berry}} = 0.58 \times 2\pi \sim 1.16\pi$ [28], corresponding to a nontrivial Berry phase. The slightly larger Φ_{Berry} (compared to π) could be due to errors in determining the minimum ΔM, where there may be another oscillation with smaller amplitude and lower frequency. However, determining this low-frequency oscillation requires further measurement above 7 T. Additionally, from the Onsager relation $F = (\Phi_0/2\pi^2)S_F$ (Φ_0 is the flux quanta), we can estimate the extreme Fermi surface area (S_F) normal to the [111] direction $\sim 0.98\,\text{nm}^{-2}$ corresponds to a small Fermi wave vector $k_F \sim 0.055\,\text{Å}^{-1}$.

To further understand the observed properties, the electronic structure is calculated using the DFT and shown in Fig. 2(a). Consistent with previous results [10], there are three bands crossing the Fermi level (E_F) with contributions from both Pd and Sb. At the R point, there is a sixfold degeneracy, marked by a circle in Fig. 2(a). Three bands are congregating at the R point as the nonsymmorphic symmetry protects this degeneracy. Since all of them are doubly degenerate due to the inversion symmetry, sixfold degeneracy exists at the R point. In addition, we find that Sb dominates the band structure around E_F (Table S1 [13]).

The above analysis indicates that the topological states near E_F at the Γ and R points are primarily coming from Sb (between -0.37 eV and E_F). The density of states (DOS) plots displayed in Fig. 2(b), show that there is a crossover at ~ -1.5 eV where the site-projected Sb DOS overtakes the Pd site-projected DOS, indicating that on the more global scale there is a larger contribution of Sb states near E_F compared to the Pd states. Furthermore, the effective masses of the three bands at the R point are much lighter than bands located at the Γ point. This indicates that the latter has higher DOS than that in the R point. Subsequently, the larger contribution of Sb than Pd to the DOS near E_F suggests that the two lightest bands at the R point are from Pd.

DFT calculations clearly show that there are both electron and hole bands across E_F. To figure out which band plays a dominant role in electrical transport, we measured the Hall resistivity (ρ_H) at various temperatures. As shown in Fig. 3(a), ρ_H exhibits linear field dependence with positive slope $R_H = \rho_H/H$ at all temperatures, implying hole-dominant charge carriers, and behaves like the single-band situation. The latter is in agreement with Kohler's scaling behavior. The hole concentration estimated through $n = \frac{1}{eR_H}$, as shown in Fig. 3(b), decreases with decreasing temperature, reaching $2.5 \times 10^{21}/\text{cm}^3$ at 2 K. The concentration of charge carriers is consistent with the good metallic behavior of $PdSb_2$ observed. According to $\mu_H = R_H/\rho$, the Hall mobility μ_H is calculated, which is shown in Fig. 3(b). With decreasing temperature, μ_H increases, reaching $380\,\text{cm}^2\ \text{V}^{-1}\ \text{s}^{-1}$ at 2 K. This value of mobility is two orders of magnitude lower than that of Cd_3As_2 ($8 \times 10^4\,\text{cm}^2\ \text{V}^{-1}\ \text{s}^{-1}$) [8]. Since the resistivity of $PdSb_2$ is lower than that of Cd_3As_2, the lower μ_H is due to the higher n in $PdSb_2$.

Since the electrical transport properties of $PdSb_2$ are governed by carriers residing in one of the hole bands at the ambient pressure, would the electronic structure change under pressure? Figures 2(c) and 2(d) show the band structure under 17.66 and 45.60 GPa respectively. While heavy bands (Γ point) remain almost intact, the degenerate light bands (R point) are gradually pushed upward. Above $\sim$17.66 GPa, the light bands no longer cross E_F, as shown in Fig. 2(d). This indicates that the DOS decreases with increasing pressure (Fig. S4 [13]). Moreover, a Bader charge analysis performed for $p = 0$ and 45.60 GPa indicates that, under pressure, Pd gains charge while Sb loses charge, although the Bader volume is larger for Sb (Table S2 [13,29–32]).

To probe the effect of the band shift with pressure, we performed the electrical resistivity measurements between 2 and 300 K under quasihydrostatic pressure up to 52 GPa. While the temperature dependence remains similar to that at ambient pressure, the magnitude of ρ tends to decrease with increasing pressure. Upon increasing p, there is little change in ρ in p_1 (=5 GPa) $< p < p_2$(=35 GPa), as seen in Figs. 4(a) and 4(b). Remarkably, above p_2, two dramatic features are observed: (1) the magnitude of ρ increases with increasing p, and (2) there is sharp resistivity drop with $p \geqslant 41$ GPa. Below, we quantitatively analyze these two features.

Under pressure, we find that ρ continuously follows T^2 temperature dependence at low temperatures. We thus fit the low-temperature $\rho(T)$ using the same formula as that for

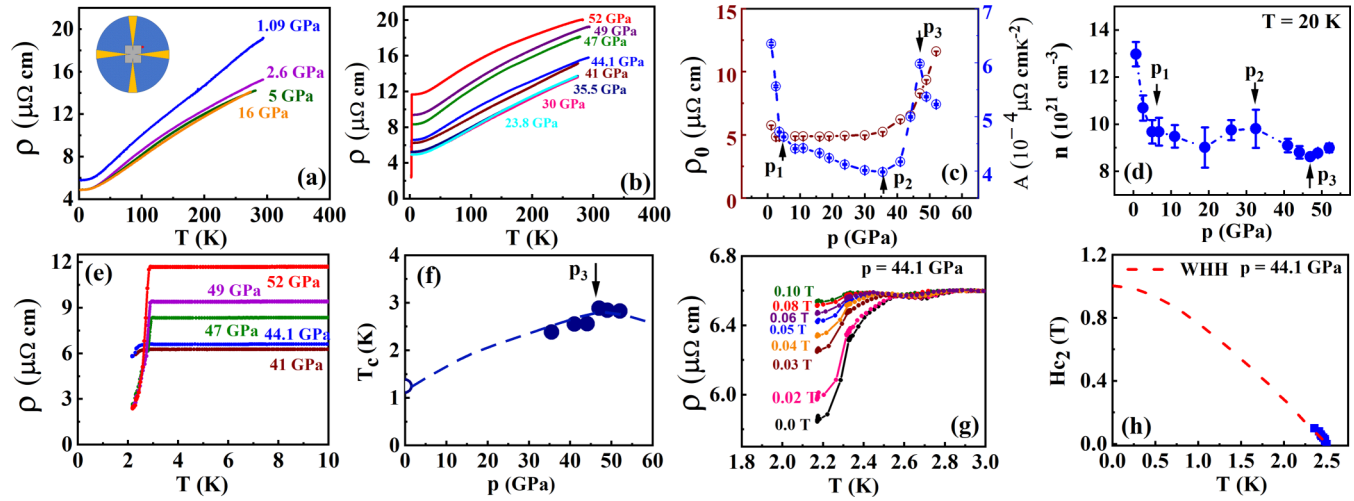

FIG. 4. (a), (b) Temperature dependence of ρ under pressure. Inset: Schematic configuration of electrodes on the sample. (c) Pressure dependence of ρ_0 and A (see text). (d) Pressure dependence of n at $T = 20$ K. (e) Temperature dependence of ρ showing superconducting transition. (f) Pressure dependence of T_c, where the dashed line is to guide the eye based on information in Ref. [12]. (g) Temperature dependence of ρ under 44.1 GPa at indicated magnetic fields. (h) Temperature dependence of H_{c2} at 44.1 GPa. The dashed line represents the WHH prediction based on the slope at $T_{c0} \sim 2.5$ K.

the ambient pressure case. Figure 4(c) displays both residual resistivity ρ_0 and coefficient A under pressure. After initial drop, ρ_0 increases with increasing p when $p \gtrsim 2.6$ GPa, with larger slope when $p > p_2$. The increase of ρ_0 with pressure may be because of the increased scattering with impurities in the squeezed environment. On the other hand, the coefficient A initially decreases then increases after reaching the minimum at p_2. It further decreases after reaching the maximum at $p_3 \sim 47$ GPa. Within the Fermi-liquid theory, A is proportional to DOS. The nonmonotonic pressure dependence of A implies the nonmonotonic variation of DOS. This suggests that the shift of sixfold-degenerate bands to higher energy by pressure [Figs. 2(c) and 2(d)] involves charge transfer, thus changing the DOS. It should be pointed out that our XRD measurements under pressure show no evidence of any structural phase transition (Fig. S3 [13,33]).

To confirm the change of DOS under pressure, we measured the pressure dependence of ρ_H at 20 K. While the field dependence of ρ_H is linear with positive slope as seen in Fig. 3(a), the slope R_H depends on p. Figure 4(d) shows the pressure dependence of n converted from R_H, which varies nonmonotonically. There is a kink at p_1, a local maximum at p_2, and a minimum at p_3. The change of n reflects electron redistribution under pressure. Given the overall similar $\rho(T)$ profile under the wide range of pressure, the dominant hole carriers should be from the doubly degenerate band starting ~ -0.6 eV at the X point that has a hole pocket between the M and Γ [Fig. 2(a)].

We now turn to the sharp resistivity drop at low temperatures and high pressure which is shown in Fig. 4(e). Note that there is an obvious drop at 41 GPa. Although not reaching zero, the resistivity drop becomes sharper under higher pressure. This suggests that the system undergoes a superconducting transition. We determine the critical temperature T_c, at which ρ reduced to 90% of its normal value. As plotted in Fig. 4(f), T_c initially increases, then decreases after reaching maximum at p_3. Since $T_c = 1.2$ K is expected at ambient pressure [12], there may be a superconducting dome as shown in Fig. 4(f).

To further check the origin of resistivity drop, we apply magnetic field at $p = 44.1$ GPa. As shown in Fig. 4(g), the resistivity drop is reduced upon the application of field, consistent with the scenario of a superconducting transition. The T_c value at each field is plotted as the upper critical field H_{c2} versus T [Fig. 4(h)]. Using the initial slope $dH_{c2}/dT|_{T=Tc0} \sim -0.58$ T/K, we further estimate the $H_{c2}(T = 0\,\text{K}) \sim 1$ T using the Werthamer-Helfand-Hohenberg (WHH) approximation [34].

In view of pressure dependence of quantities shown in Fig. 4, one may note that at p_3, T_c and A reach the maximum while n reaches the minimum. This implies that strong electron-electron interactions (large A) in the environment of reduced carrier concentration favor superconductivity. Within the BCS theory, T_c is determined by the Debye frequency, DOS, and electron-phonon coupling strength. Since the $\rho(T)$ profile is unchanged over a wide temperature range, we may assume that there is no dramatic change in Debye frequency with pressure. This again points to the electronic origin for superconductivity.

In conclusion, we have successfully synthesized high-quality $PdSb_2$ single crystals with the nonsymmorphic symmetry. Our first-principles calculations confirm that $PdSb_2$ hosts sixfold-degenerate fermions with a degeneracy stabilized by the nonsymmorphic symmetry. By applying field along the high-symmetry [111] direction, de Haas–van Alphen oscillations with $F = 102$ T are observed, corresponding to a band hosting electrons with nearly zero effective mass ($0.045m_0$) and a nontrivial Berry phase (1.16π). In addition to large and nonsaturated magnetoresistance under magnetic field, the application of quasihydrostatic pressure

modifies the electronic structure and changes superconducting transition temperature with $T_c^{max} \sim 2.9\,K$ at $p_3 \sim 47\,GPa$. Interestingly, the normal-state resistivity under pressure behaves similarly to that at ambient pressure, and follows Fermi-liquid behavior at low temperatures prior to the entrance of superconducting state. At T_c^{max}, the coefficient A shows the maximum as well, while the carrier concentration reaches minimum. This suggests that the formation of Cooper pairs (bosons) is the consequence of strong electron-electron interaction. Our discovery of nearly massless electrons with nontrivial Berry phase and superconductivity in a sixfold-degenerate material offers a unique system to study the behavior of both fermions and bosons.

This material is based upon work supported by the U.S. Department of Energy under EPSCoR Grant No. DE-SC0012432 with additional support from the Louisiana Board of Regents. The high-pressure experiment at Institute of Physics, Chinese Academy of Sciences was supported by China NSF and MOST research projects.

R.C. and Y.J. contributed equally to this work.

[1] Z. K. Liu, B. Zhou, Y. Zhang, Z. J. Wang, H. M. Weng, D. Prabhakaran, S.-K. Mo, Z. X. Shen, Z. Fang, X. Dai *et al.*, Science **343**, 864 (2014).

[2] V. Mourik, K. Zuo, S. M. Frolov, S. R. Plissard, E. P. A. M. Bakkers, and L. P. Kouwenhoven, Science **336**, 1003 (2012).

[3] B. Q. Lv, H. M. Weng, B. B. Fu, X. P. Wang, H. Miao, J. Ma, P. Richard, X. C. Huang, L. X. Zhao, G. F. Chen *et al.*, Phys. Rev. X **5**, 031013 (2015).

[4] B. Q. Lv, Z.-L. Feng, Q.-N. Xu, X. Gao, J.-Z. Ma, L.-Y. Kong, P. Richard, Y.-B. Huang, V. N. Strocov, C. Fang *et al.*, Nature (London) **546**, 627 (2017).

[5] P. B. Pal, Am. J. Phys. **79**, 485 (2011).

[6] D. Singh, N. Mobed, and G. Papini, Phys. Rev. Lett. **97**, 041101 (2006).

[7] S. Huang, J. Kim, W. A. Shelton, E. W. Plummer, and R. Jin, Proc. Natl. Acad. Sci. USA **114**, 6256 (2017).

[8] T. Liang, Q. Gibson, M. N. Ali, M. Liu, R. J. Cava, and N. P. Ong, Nat. Mater. **14**, 280 (2014).

[9] M. Yan, H. Huang, K. Zhang, E. Wang, W. Yao, K. Deng, G. Wan, H. Zhang, M. Arita, H. Yang *et al.*, Nat. Commun. **8**, 257 (2017).

[10] B. Bradlyn, J. Cano, Z. Wang, M. G. Vergniory, C. Felser, R. J. Cava, and B. A. Bernevig, Science **353**, 5037 (2016).

[11] S. Furuseth, K. Selte, and A. Kjekshus, Acta Chem. Scand. **19**, 735 (1965).

[12] B. T. Matthias, T. H. Geballe, and V. B. Compton, Rev. Mod. Phys. **35**, 1 (1963). $PdSb_2$ is listed within as a superconductor with $T_c = 1.2\,K$. However, there are no data to support such claim.

[13] See Supplemental Material at http://link.aps.org/supplemental/10.1103/PhysRevB.99.161110 for the sample growth process, crystal structure, and magnetization, comparison of transverse and longitudinal MR, characterization under pressure, band-structure calculations, and site contribution to the wave function at Γ and R points of the Brillouin zone (which includes Refs. [15,18,29–33]).

[14] N. E. Brese and H. G. Schnering, Z. Anorg. Allg. Chem. **620**, 393 (1994).

[15] H. K. Mao, J. Xu, and P. M. Bell, J. Geophys. Res. **91**, 4673 (1986).

[16] J. L. Zhang, S. J. Zhang, H. M. Weng, W. Zhang, L. X. Yang, Q. Q. Liu, S. M. Feng, X. C. Wang, R. C. Yu, L. Z. Cao *et al.*, Proc. Natl. Acad. Sci. USA **108**, 24 (2011).

[17] S. J. Zhang, J. L. Zhang, X. H. Yu, J. Zhu, P. P. Kong, S. M. Feng, Q. Q. Liu, L. X. Yang, X. C. Wang, L. Z. Cao *et al.*, J. Appl. Phys. **111**, 112630 (2012).

[18] J. P. Perdew, K. Burke, and M. Ernzerhof, Phys. Rev. Lett. **77**, 3865 (1996).

[19] G. Kresse and J. Furthmüller, Phys. Rev. B **54**, 11169 (1996).

[20] G. Kresse and D. Joubert, Phys. Rev. B **59**, 1758 (1999).

[21] P. E. Blöchl, Phys. Rev. B **50**, 17953 (1994).

[22] F. J. Blatt, *Physics of Electronic Conduction in Solids* (McGraw-Hill, New York, 1968).

[23] A. A. Abrikosov, *Fundamentals of the Theory of Metals* (North-Holland, Oxford, 1988).

[24] S. W. Van Sciver, in *Helium Cryogenics. The International Cryogenics Monograph*, edited by K. D. Timmerhaus and C. Rizzuto (Springer, Boston, 1986).

[25] A. B. Pippard, *Magnetoresistance in Metals* (Cambridge University Press, Cambridge, England, 1989).

[26] A. Narayanan, M. D. Watson, S. F. Blake, N. Bruyant, L. Drigo, Y. L. Chen, D. Prabhakaran, B. Yan, C. Felser, T. Kong *et al.*, Phys. Rev. Lett. **114**, 117201 (2015).

[27] I. M. Lifshitz and A. M. Kosevich, Sov. Phys. JETP **2**, 636 (1956).

[28] D. Shoenberg, *Magnetic Oscillations in Metals* (Cambridge University Press, Cambridge, England, 2009).

[29] W. Tang, E. Sanville, and G. Henkelman, J. Phys.: Condens. Matter **21**, 084204 (2009).

[30] E. Sanville, S. D. Kenny, R. Smith, and G. Henkelman, J. Comput. Chem. **28**, 899 (2007).

[31] G. Henkelman, A. Arnaldsson, and H. Jónsson, Comput. Mater. Sci. **36**, 354 (2006).

[32] M. Yu and D. R. Trinkle, J. Chem. Phys. **134**, 064111 (2011).

[33] A. P. Hammersley, S. O. Svensson, M. Hanfland, A. N. Fitch, and D. Hausermann, High Pressure Res. **14**, 235 (1996).

[34] N. R. Werthamer, E. Helfand, and P. C. Hohenberg, Phys. Rev. **147**, 295 (1966).